The *POF1B* candidate gene for premature ovarian failure regulates epithelial polarity

Valeria Padovano[1], Ilaria Lucibello[1], Valentina Alari[1], Pamela Della Mina[2], Arianna Crespi[1], Ilaria Ferrari[1], Marta Recagni[1], Donatella Lattuada[1], Marco Righi[1,3], Daniela Toniolo[4], Antonello Villa[2] and Grazia Pietrini[1,3,*]

[1]Department of Pharmacology, Medical School, Università degli Studi di Milano, 20129 Milan, Italy
[2]Consorzio MIA, Università Milano-Bicocca, 20052 Monza, Italy
[3]CNR- Institute of Neuroscience, 20129 Milan, Italy
[4]Division of Genetics and Cell Biology, San Raffaele Scientific Institute, 20132 Milan, Italy
*Author for correspondence (grazia.pietrini@unimi.it)

Accepted 27 May 2011
Journal of Cell Science 124, 3356–3368

doi: 10.1242/jcs.088237

Summary

POF1B is a candidate gene for premature ovarian failure (POF); it is mainly expressed in polarised epithelial tissues, but its function in these tissues and the relationship with the disorder are unknown. Here we show colocalisation of POF1B with markers of both adherens and tight junctions in human jejunum. The tight junction localisation was maintained by the human POF1B stably expressed in the MDCK polarised epithelial cell line, whereas it was lost by the POF1B R329Q variant associated with POF. Localisation of apico-basal polarity markers and ultrastructure of the tight junctions were maintained in cells expressing the mutant. However, tight junction assembly was altered, cells were dysmorphic and the monolayer organisation was also altered in three-dimensional culture systems. Moreover, cells expressing the POF1B R329Q variant showed defects in ciliogenesis and cystogenesis as a result of misorientation of primary cilia and mitotic division. All of these defects were explained by interference of the mutant with the content and organisation of F-actin at the junctions. A role for POF1B in the regulation of the actin cytoskeleton was further verified by shRNA silencing of the endogenous protein in human intestinal Caco-2 cells. Taken together, these data indicate that localisation of POF1B to tight junctions has a key role in the organisation of epithelial monolayers by regulating the actin cytoskeleton.

Key words: Cell shape, Epithelial polarity, F-actin, Primary cilia, Tight junctions, 3D multi-lumen cyst, POF1B shRNA

Introduction

Premature ovarian failure (POF) or premature menopause affects 2–3% of women and is characterised by primary and secondary amenorrhea, owing to the cessation of ovarian function before the age of 40 years, associated with hypoestrogenism and high serum gonadotropins levels. POF is usually idiopathic or sporadic (Coulam et al., 1986), but the role of familial factors is suggested by the frequent finding of familial cases (de Moraes-Ruehsen and Jones, 1967). On the basis of five kindreds, it has been proposed that POF may be a mendelian disorder, inherited paternally or maternally as an autosomal or X-linked dominant trait (Mattison et al., 1984).

Cytogenetic studies of X chromosome aberrations have identified a 'critical region' for normal ovarian function that is mainly within the long arm of the X chromosome (Krauss et al., 1987; Bione et al., 1998; Davis et al., 2000). Four candidate genes have been found to be interrupted by an X;1 balanced translocation in this critical region, and *POF1B* was first identified in a patient presenting secondary amenorrhea at the age of 17 years (Riva et al., 1996). *POF1B* maps to the Xq21 region, and the presence of a homologue on the Y chromosome has been excluded (Bione et al., 2004). Moreover, it escapes X chromosome inactivation, which suggests that this region contains a gene that is essential to ovarian function but might be mutated in some non-deletion cases and lead to the same clinical picture of premature ovarian failure. A recent study of a Lebanese family with POF showing linkage to Xq21 identified a G-to-A transition at nucleotide 1132 in exon 10 of the gene that resulted in an Arg-to-Gln (R329Q) mutation. The affected family members were homozygous (Lacombe et al., 2006).

POF1B is an evolutionary novel gene found only in vertebrates. It has a large coiled-coil region in the C-terminal half of the protein (aa 332–532) that shows significant homology to the C-terminal coiled-coil domain of barmotin/7H6 (Rizzolio et al., 2007), a tight-junction-associated protein, and to the myosin heavy chain rod domain (from residues 629–870 of the consensus sequence of the myosin rod domain) (Lacombe et al., 2006). In vitro assays have shown that POF1B binds to non-muscle actin filaments, whereas the binding affinity of the POF1B R329Q variant is greatly diminished (Lacombe et al., 2006). Interestingly, POF1B is highly expressed in polarised epithelial tissues characterised by the presence of tight junctions (TJs) (Rizzolio et al., 2007); these junctions exert a barrier function by restricting paracellular permeability through the epithelial layers, a task that mainly relies on the ability to organise an appropriate actin junctional cytoskeleton. In line with a role in these junctions, the expression of POF1B during mouse development is activated in the external layers of the epidermis just before the formation of the epidermal permeability barrier (Rizzolio et al., 2007). However, there are no published data concerning the localisation and potential role of POF1B in tight

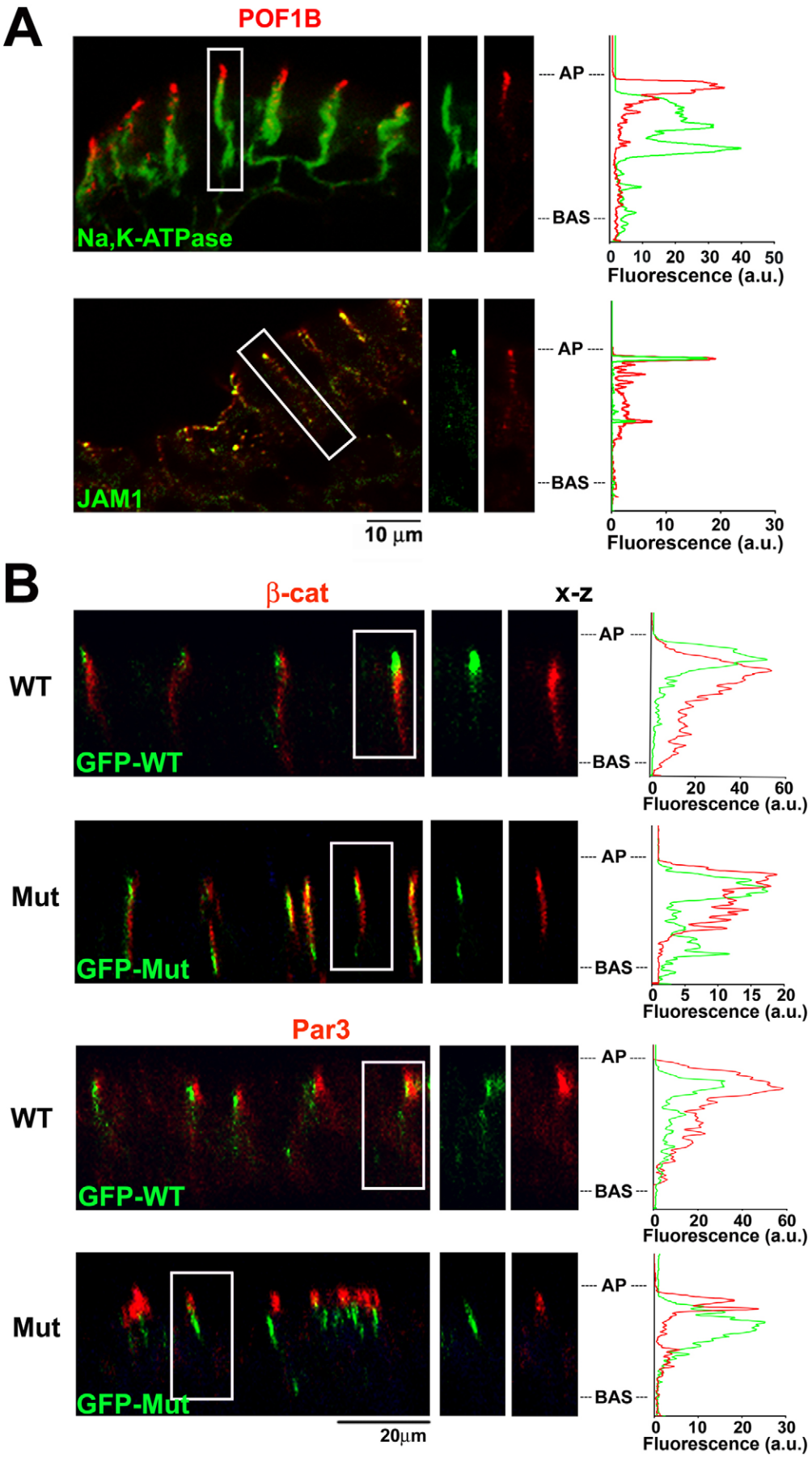

Fig. 1. POF1B R329Q fails to localise to TJs in fully polarised MDCK cells. (**A**) Confocal analysis of immunofluorescence double staining for POF1B (red) and the Na^+/K^+-ATPase marker of adherens junctions or the JAM1 marker of tight junctions in human jejunum (green). (**B**) Immunofluorescence analyses of MDCK cells stably expressing wild-type GFP–POF1B (WT) or GFP–POF1B R329Q (Mut). Cells grown at confluency for >3 days in Transwell filters were double stained for the indicated markers and analysed by confocal microscopy. Vertical (*x–z*) confocal sections are stained for the β-catenin marker of AJs (β-cat) and the Par3 marker of TJs (red). POF1B localisation is revealed by GFP fluorescence (green). (A,B) Red and green pixel intensity along the lateral surface of the corresponding images is expressed in fluorescence arbitrary units (a.u.). AP, apical region; BAS, basal region.

junctions, or the effects of the R329Q mutation on epithelial polarity.

We investigated the localisation of POF1B in human jejunum, as well as the localisation of the human wild-type and mutant protein in the MDCK cell model of polarised epithelial cells stably transfected with the cDNAs encoding POF1B or the POF1B R329Q variant, respectively. The effects of the overexpression of these proteins on TJ assembly were investigated by means of morphological and functional analyses. Defects during the acquisition of surface polarity were evaluated in cells grown to confluence on Transwell filter supports (two-dimensional cultures, 2D) and in organotypical three-dimensional (3D) cultures using laser confocal and electron microscopy. The organisation of the actin cytoskeleton was analysed qualitatively (morphological and biochemical assays) and quantitatively (FACS analysis). Moreover, the function of POF1B in the regulation of actin dynamics was verified by silencing the endogenous protein in the human intestinal Caco-2 cell line.

Results

The R329Q substitution prevents the localisation of POF1B to tight junctions

The specific spatial and temporal expression in gastrointestinal tracts and granular layer of the epidermis has led to the suggestion that POF1B has a role in the acquisition and/or maintenance of epithelial polarity (Rizzolio et al., 2007). Because TJs are the most relevant junctions for acquisition and maintenance of the polarised phenotype, we first investigated the TJ localisation of endogenous POF1B in human jejunum (Fig. 1A), using specific antibodies against POF1B (red) and Na^+/K^+-ATPase, which is a marker of the lateral surface, or JAM1, a TJ marker (green). POF1B localises along the entire lateral junctional domain. Staining was punctuated along the surface homogenously labelled by the Na^+/K^+-ATPase antibody. A yellow colour indicating the colocalisation was not seen in the merged image because the green staining of the pump was predominant; however, the red staining of POF1B was clearly enriched in a more apical region of the lateral surface that is devoid of Na^+ pumps (Fig. 1A, see the lack of overlap between the green and red peak of fluorescence in the apical position). The green JAM1 staining was enriched in an apical portion of the lateral junctional domain and the colocalisation with POF1B was revealed by the yellow staining and by the overlap of the fluorescence peaks. These data indicate a localisation of POF1B along the entire lateral junctional surface, and its enrichment at the level of the tight junctions in human jejunum.

We then investigated the effects of overexpression of full-length POF1B (WT) and its R329Q variant (Mut) on the surface polarisation of epithelial cells. To this end, we stably expressed the cDNAs fused to the green fluorescent protein (GFP) in the MDCK polarised epithelial cell line, a cell model that is widely used to study the role of polarity proteins. At least three independent WT and Mut clones were selected and the localisation of the transfectant characterised by confocal and western blot analysis (Figs 1, 2). Vertical confocal sections (x–z) showed a similar distribution of POF1B to that observed in human jejunum, and the localisation of the WT (green staining) construct extended beyond the staining of the β-catenin (red staining) marker of adherens junctions (AJs). The localisation of POF1B at the cytoplasmic face of TJs was further confirmed by its colocalisation with the Par3 marker of this domain (Fig. 1B, compare the green peak with the red of β-catenin or with that of Par 3). By contrast, the localisation of Mut did not extend in the apical direction beyond that of β-catenin, and the mutant did not colocalise with Par3 at the TJ level (Fig. 1B, see the almost complete overlap between the Mut peak with that of β-catenin but not with Par3).

Apico-basal polarity is maintained in MDCK cells expressing POF1B R329Q

The effects of POF1B overexpression on polarity markers was investigated by western blot analysis in MDCK cell lysates. Approximately a threefold reduced expression of the apical marker gp135 and the tight junctional marker claudin-2 (Cla2) was revealed in Mut cells (Fig. 2A,B). However, claudin-2 and gp135, as well as all the junctional polarity markers tested maintained their specific surface localisation (Fig. 2C), thus suggesting that apico-basal polarity is maintained in Mut cells. The reduced expression of these markers was not due to variability among the cell lines, because it was observed in three independent clones, and it was associated with the level of expression of the transfectants, whereas significant changes in the expression of other markers were not confirmed (data not shown).

Because claudins influence the charge selectivity and electrical resistance of junctions, we measured transepithelial electrical resistance (TER) (Fig. 2D) and paracellular permeability to FITC-Dextran (not shown). WT cell monolayers grown at confluency for more than 5 days showed significantly higher TER values than control MDCK cells or MDCK cells transfected with the variant. Incubation with a low-calcium medium to disassemble the junctions abolished TER in all of the cells, whereas the replacement with regular medium induced junction reassembly. The WT-expressing cells peaked earlier than untransfected MDCK cells, whereas the TER peak was virtually absent in cell lines expressing the mutant. However, apico-basal polarity and steady-state TER in Mut cells were not affected, and the altered TER acquisition profile did not correlate with an increased permeability of FITC-Dextran (data not shown), suggesting that POF1B R329Q does not interfere with TJ barrier properties for large solutes.

Altered organisation of the monolayer in MDCK cells expressing POF1B R329Q

No remarkable differences in TJ ultrastructure in cells expressing the different constructs were observed by means of conventional electron microscopy (data not shown). The ultrastructural analysis, however, revealed that the MDCK monolayer expressing the mutant contained cells of various shapes and sizes that sometimes appeared as a pseudostratified monolayer (Fig. 3A), although these cells were still capable of forming morphologically normal junctions, as shown by the presence of TJs in highly dysmorphic cells (Fig. 3B).

Defects in cell size and monolayer organisation were also observed by confocal analysis of Mut distribution. POF1B and POF1B R329Q were particularly enriched at sub-apical and basal levels (Fig. 3C,D), although the latter staining was more discontinuous (compare sub-apical and basal staining in 3D image reconstructions and horizontal sections), and thus rarely seen in vertical sections (Fig. 1B). The enrichments were resolved as two rings, one at the sub-apical and the other at the basal level in both horizontal sections (x–y) and 3D

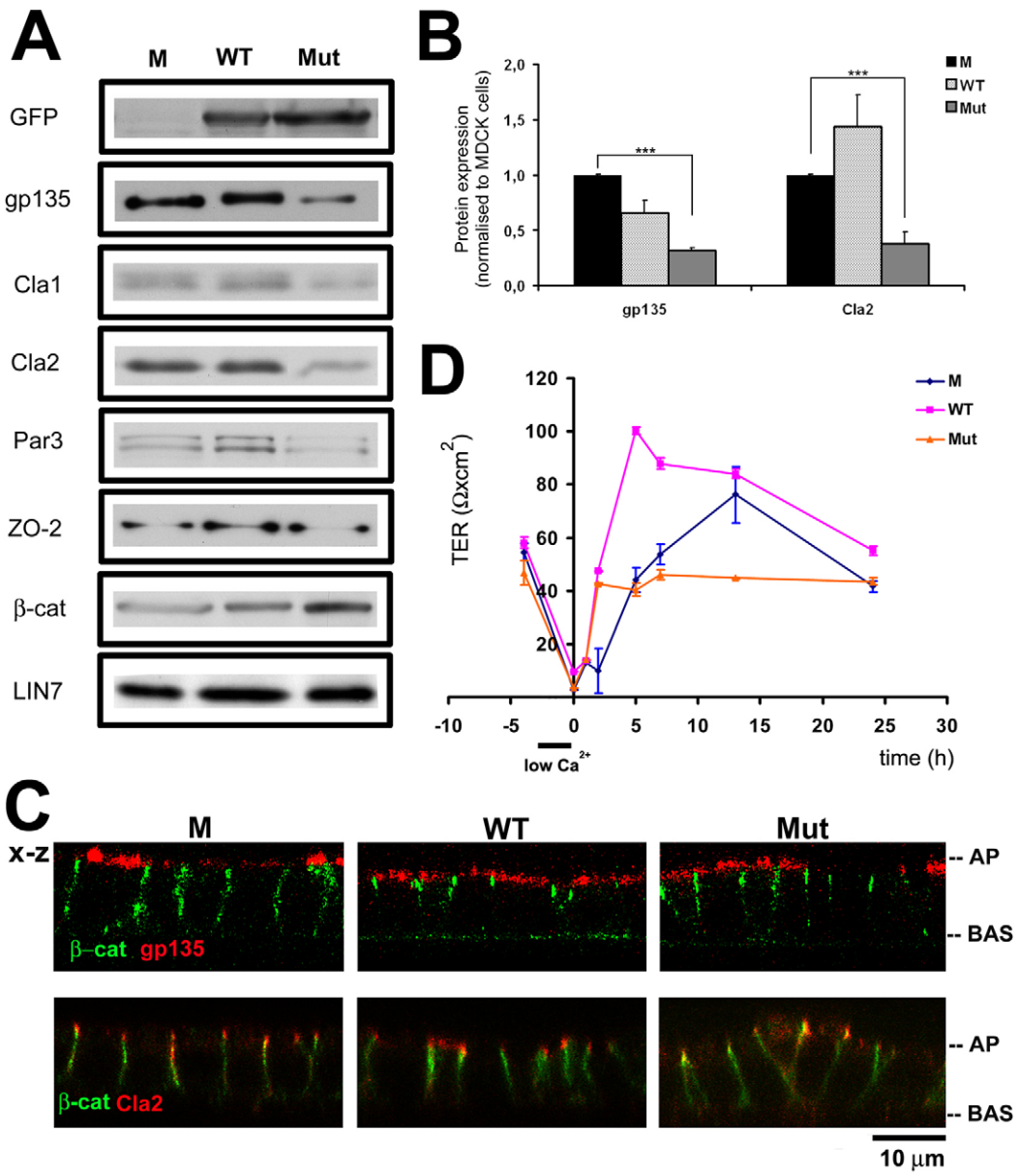

Fig. 2. Altered mechanism of TER acquisition in POF1B R329Q cells. (**A**) A representative western blot analysis of the total expression of junctional markers in control MDCK cells (M), MDCK cell lines overexpressing GFP–POF1B or GFP–POF1B R329Q. Equal amounts of cell extracts were loaded onto 10% SDS-PAGE and the transferred proteins were immunoprobed for GFP (to quantify the expression of the WT and Mut constructs in the cell lines) and markers of the apical surface (gp135), tight junctions (Cla1, Cla2, Par3, ZO-2 and LIN7) and adherens junctions (β-cat and LIN7). (**B**) Quantification of the expression of gp135 and Cla2 in transfected and untransfected cells. The results are the means ± s.e.m. of three independent experiments performed in control, and two stable clones for WT and Mut; one of these experiments, normalised to control MDCK cells, is shown in A (***$P<0.001$). (**C**) Vertical confocal sections (x–z) of double immunofluorescence staining for β-catenin (green) and the apical marker gp135 or the tight junctional marker Cla2 (red) in control (M) and transfected (WT or Mut) MDCK cells. AP: apical surface; BAS: basal surface. (**D**) TER assay in control (M), WT and Mut cell lines. Cell monolayers grown at confluence for more than five days on Transwell filters were incubated with low calcium medium (low Ca^{2+}) to disassemble the junctions (TER=0). Junction reassembly induced by calcium replacement was followed by measuring TER at the indicated times. Each value ± s.e.m. represents the average of three experiments performed in two stable clones.

reconstructions (Fig. 3C,D, see supplementary material Movies 1 and 2). Low levels of POF1B were found between the apical and basal enrichments, whereas the mutant protein showed a more diffuse localisation between the two rings, which in 3D-images, partially masked the lower ring.

In horizontal sections of Mut monolayers, we noticed that more than three cells often contacted each other at a single point (Fig. 3D, vertices, compare the red masks drawn on WT and Mut sub-apical sections) and the number of hexagonal cells was considerably reduced, whereas the number of cells with four sides increased threefold (Fig. 3E). Moreover, Mut cells showed a greater variability in the length of their sides (mean value, 7.80±0.15 μm) and the percentage of angles between 100 and 140 degrees was significantly reduced (the ideal measure of each angle

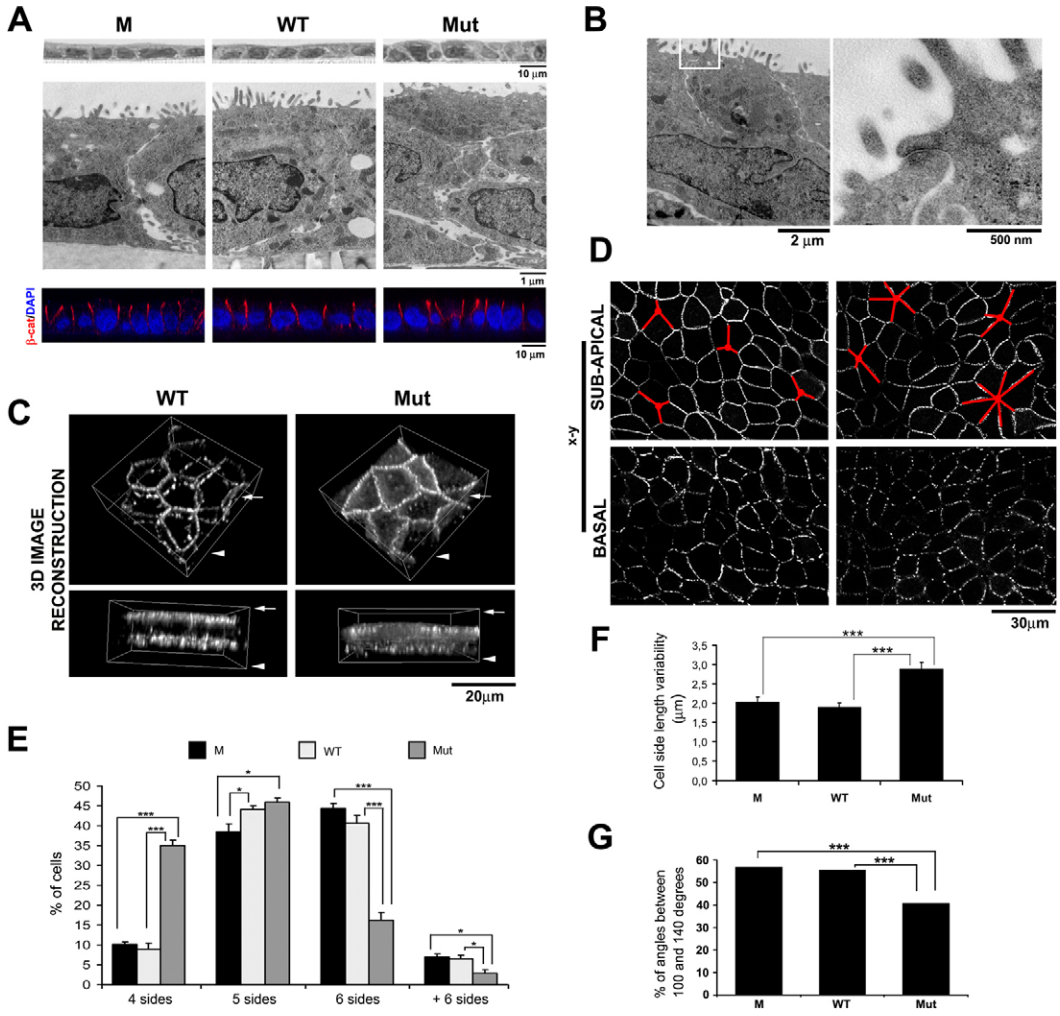

Fig. 3. Altered cell morphology and monolayer organisation in cells expressing POF1B R329Q. Control MDCK cells (M), MDCK cell lines transfected with POF1B (WT) or POF1B R329Q (Mut) were grown confluent on Transwell filters for >3 days and processed for EM or immunofluorescence. (**A**) Semithin sections (top), TEM images (middle) and immunofluorescence staining (bottom) using the β-catenin antibody (red) and DAPI (blue). (**B**) Ultrastructural analysis in highly dysmorphic Mut cells; a 4 × magnification is shown on the right. (**C**) Immunofluorescence analysis of POF1B localisation. Tilted volume rendering of entire volume of cells (3D-image reconstructions) showing 3D apical (upper) and side (lower) views of a group of cells. Arrows and arrowheads indicate the apical and basal region of the cell monolayer, respectively. (**D**) Horizontal (*x*–*y*) confocal sections of POF1B localisation in WT and Mut cell lines taken at the sub-apical and basal region of the cell monolayers. A red mask is drawn on sub-apical sections to highlight cell arrangement in the monolayer. (**E**) Quantification of cells with four (quadrilateral), five (pentagonal), six (hexagonal) or more than six sides (n=350 for each cell line). (**F**) Cell side length variability was measured within each cell on an average of 50 cells in at least three different experiments. (**G**) Angles measured in 100 cells per each cell line using a macro developed in ImageJ (see the Materials and Methods). Data in E–G are the means ± s.e.m. of three independent experiments performed with two stable clones for each transfectant. *P<0.05; **P<0.01; ***P<0.001.

if three cells contact each other at a single point is 120 degrees) (Fig. 3F,G). It is known that epithelial cells tend to pack into regular hexagons to reach a thermodynamically favourable state and so an increased divergence from the shape of regular polygons in which all angles are equal in size and all sides have the same length (equiangular and equilateral polygon) is a clear sign of a perturbed organisation of the monolayer (Carthew, 2005).

Decreased levels and altered organisation of F-actin in MDCK cells expressing POF1B R329Q

Irregularity of cell shape, which disturbs the monolayer polarity, might be a consequence of dysfunctional POF1B. Because cell shape and specialised cellular functions depend on an underlying network of dynamic actin polymers (F-actin) that ensure mechanical stability and flexibility of the cortex (Van Itallie et al., 2009), we analysed the effects of POF1B expression on the actin cytoskeleton.

We first verified that both POF1B apical and basal rings contained F-actin in 3D reconstructions of cells stained with phalloidin to detect F-actin (Fig. 4A, yellow, only colocalisation signals were represented). Note that the distribution of POF1B (WT and Mut) is maintained, but the Mut distribution appeared more diffuse along the entire lateral surface and less enriched at the apical ring (compare with the 3D images in Fig. 3B), suggesting a major overlap between F-actin and WT, as compared with Mut. Because confluent MDCK cells had an

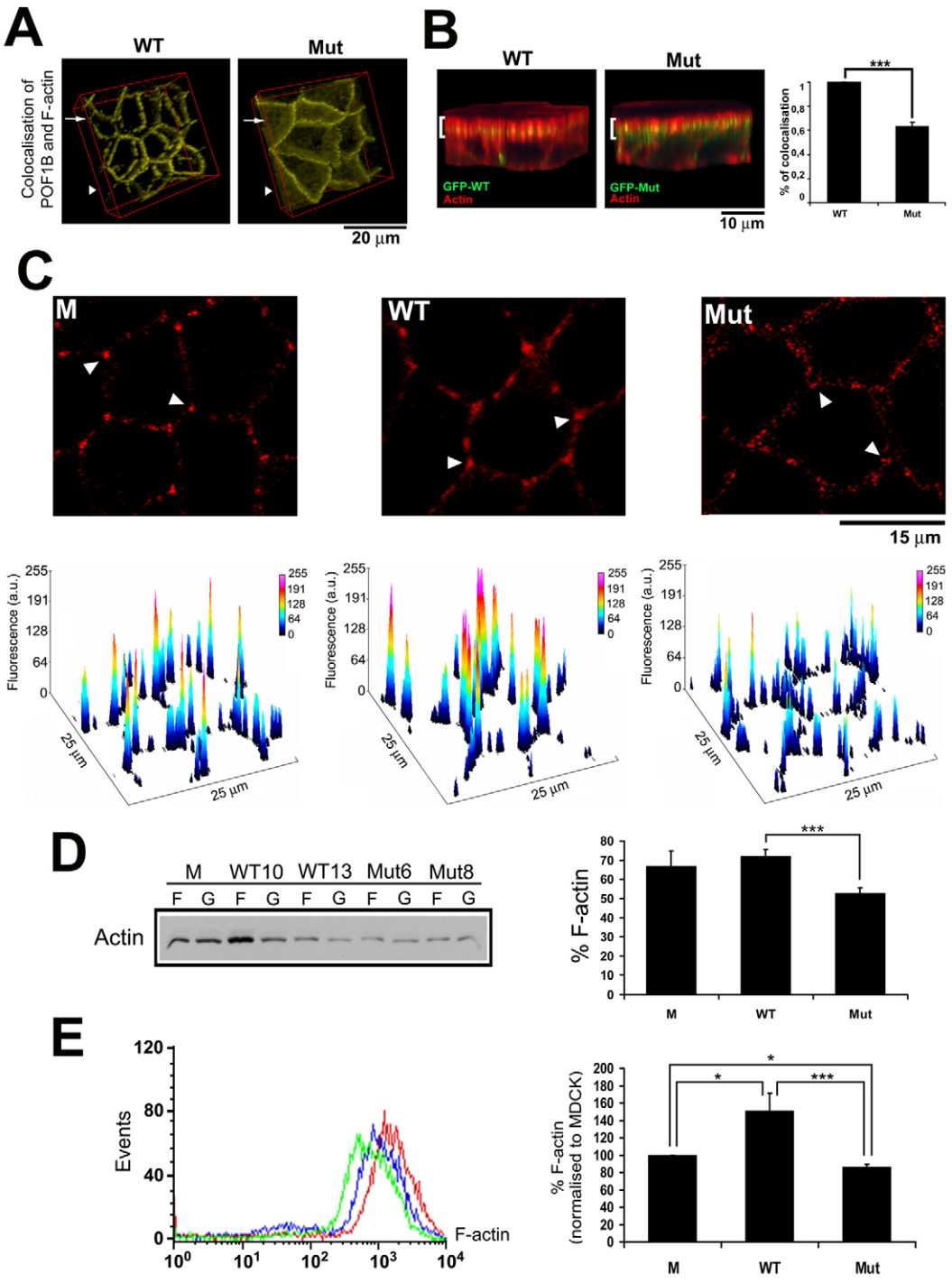

Fig. 4. F-actin defects in cells expressing POF1B R329Q. Cells grown confluent on Transwell filters (A–C), or Petri dishes (D,E) for >4 days were stained for labelled phalloidin (A–C,E) and analysed as indicated. (**A**) 3D image reconstruction representing colocalisation of POF1B and labelled phalloidin (yellow). POF1B and F-actin not colocalising are not considered. (**B**) 3D side view (left) and quantification of the percentage of POF1B and phalloidin colocalisation (right) evaluated by Manders' colocalisation coefficients in the apical region of the cells (brackets) ($n=10$ cells analysed for each stable cell line; ***$P<0.001$). (**C**) Horizontal confocal sections (upper) and their corresponding surface plot analysis (lower); the fluorescence intensity is expressed in arbitrary unit (a.u.). (**D**) A representative detergent extraction experiment. Equal volumes of insoluble F- and soluble G-fractions were loaded onto 10% SDS-PAGE and blotted into nitrocellulose; the amount of actin in each fraction was evaluated using specific antibodies (left). Quantification showing mean ± s.e.m. of three independent experiments is presented in the right panel. ***$P<0.001$. (**E**) A representative graph of F-actin signals in WT (red), Mut (green) and control MDCK cells (blue), and F-actin content comparison in transfected (WT and Mut) and untransfected (M) (set to 100%) cell lines, as determined by FACS analysis. Data represent mean ± s.e.m. of three independent experiments performed with at least two stable clones for each transfectant. *$P<0.05$; ***$P<0.001$.

apical actin cytoskeleton ring that included and circumscribed the microvilli, which was located at the same level of the apical junctions (TJs and AJs), we analysed whether WT and Mut codistributed with the apical actin in 3D side reconstructions of the indicated regions (Fig. 4B). The apical ring of WT POF1B was completely embedded into the F-actin apical enrichment, whereas the Mut staining was partially underneath the phalloidin staining of F-actin, further suggesting the exclusion of Mut from apical junctional domains. A twofold increase in colocalisation of WT and phalloidin (99%) compared with that of Mut (63.2%) was measured using Manders' colocalization coefficients (Fig. 4B, histogram).

A different distribution and content of F-actin was also observed at cell–cell contacts in Mut cells; F-actin showed a spot-like distribution along the adhesion surface and the staining was particularly marked in three-cell vertices (vertices at which three cells and three sides meet) in control cells and cells expressing WT POF1B, but not in Mut cells, (Fig. 4C, see arrowheads). Peaks of fluorescence in Mut cells, obtained using ImageJ surface plot analysis, were also lower in intensity (mainly in the blue range of the scale, whereas peaks of fluorescence in WT reach the red range of intensity) in the vertices. No significant difference was observed in apical and basal actin in Mut cells.

The effect of WT or Mut expression on F-actin was then qualitatively analysed by measuring the F-actin to G-actin ratio (Fig. 4D), and the F-actin content was quantified by FACS analysis (Fig. 4E). The ratio assay is based on the differential extractability of F-actin and G-actin from cells by detergent (Blikstad and Carlsson, 1982). In these experiments, actin was mainly found in the detergent-insoluble F-actin fraction (70%) in control and WT MDCK cells, whereas only 50% of the cellular actin was found in the F-actin fraction in Mut cells. Moreover, FACS analysis revealed a 40% increase and a 20% decrease in F-actin content, respectively in WT and Mut cells, when compared with control MDCK cells. This result supports a role for POF1B in the stabilisation of F-actin at cell–cell contacts and suggests that the mutant interferes with this process.

Actin dynamic defects in Caco-2 cells expressing POF1B shRNA

To verify the physiological role of POF1B on actin dynamics, we silenced the endogenous protein in human intestinal Caco-2 cells by transient transfection of shRNA1 and shRNA2 against POF1B (see the Materials and Methods); MDCK cells were not used in these experiments because the antibody does not cross-react with the canine protein. Similarly to MDCK cells, endogenous POF1B in Caco-2 cells localises at the apical region of the junctional domain devoid of Na^+/K^+-ATPase (Fig. 5A). Approximately 30–35% of the endogenous POF1B in Caco-2 cell lysates was silenced using both shRNAs (Fig. 5B), and this value agreed with the percentage of transfected cells (assessed by measuring the percentage of GFP-expressing cells). Cells silenced for POF1B (green), showed a decreased staining for phalloidin (Fig. 5C) and a ~20% reduction in F-actin, as quantified by FACS analysis (Fig. 5D). Moreover, cells silenced for POF1B completely lost their epithelial morphology and eventually detached from the monolayer when cultured for longer than 3 days (Fig. 5E), thus we were never able to select stable clones. Because the apico-basal polarity was maintained in cells expressing the mutant but not in POF1B-silenced cells, these results indicate a key role for POF1B in the regulation of the actin cytoskeleton that is partially retained by the mutant.

Altered ciliogenesis and cystogenesis in MDCK cells expressing POF1B R329Q

In a variety of cell systems, cytoskeleton arrangements are regulated by the tissue polarity or planar cell polarity (PCP) pathway. PCP corresponds to a secondary axis of polarity that is perpendicular to the apico-basal direction (Simons and Mlodzik, 2008; Song et al., 2010), and that is crucial for the appearance of highly organised cellular structures, such as primary cilia, as well as for the orientation of cell division. Primary cilia are sensory microtubule-based structures emanating from the apical surface of many cells, including MDCK cells (Singla and Reiter, 2006), stained by antibody against acetylated tubulin (Fig. 6A). In our experimental conditions, not all the cells in untransfected and transfected monolayers exhibited primary cilia, but the number of ciliated cells appeared markedly increased in the cell lines expressing the POF1B mutant protein (Fig. 6B). Because a direct link between actin dynamics and ciliogenesis has been documented (Kim et al., 2010), the altered organisation of the actin cytoskeleton observed in Mut cells could account for the increased number of ciliated cells. Moreover, in these cells, we noticed that cilia emerged from the apical surface at a more variable distance from their centre. Statistically, about twice as many cilia emerged closer than 2 μm from the cellular centre in WT and M cells, as compared with cilia in Mut cells (Fig. 6C, histogram). The occasional close proximity of cilia, emerging near the cell boundaries, might hence explain the appearance of interlaced cilia tips in Mut-expressing cells (Fig. 6A, arrows).

Primary cilia are microtubule-based structures guided by basal bodies that originate from and have a substructure similar to centrioles. Interestingly, the symmetrical division of epithelial cells to generate two identical daughter cells depends on the correct positioning of centrioles (Jaffe et al., 2008; Hao et al., 2010; Qin et al., 2010; Rodriguez-Fraticelli et al., 2010; Zheng et al., 2010), suggesting possible defects in the orientation of cell division in Mut cells. These defects are better visualised in the organotypical 3D extracellular matrix cell culture system (Vieira et al., 2006). Mut cells were plated into matrigel and 4-day-old cysts were stained for DAPI to localise mitotic chromosomes (Fig. 7A). As expected, cell division occurred in a direction parallel to the plane of the cyst apical surface in WT and untransfected MDCK cells (Fig. 7A, arrows), thus generating cells that maintain the polarity of the monolayer. Conversely, mitotic chromosomes were mislocalised in Mut cysts, with a large fraction of Mut cells (approximately 50%) that were not dividing in a direction parallel to the cyst surface. As a consequence, the monolayer will not be maintained and daughter cells will be forced to stratify or to form a new lumen (Fig. 7A). Misorientation of mitotic spindles is known to lead to cysts with multiple lumens (Zegers et al., 2003; Mostov et al., 2005; Jaffe et al., 2008; Zheng et al., 2010) and, indeed, we observed a higher percentage of cysts with multiple lumens or no lumens in a period up to 5 days in Mut-expressing cells (Fig. 7C). By contrast, overexpression of POF1B did not interfere with the development of spherical cysts with a single central lumen and a monolayer of cells with correctly polarised apical (facing the lumen) and lateral proteins, as shown by β-catenin and gp135 staining (Fig. 7B), respectively, in 4-day-old cysts. Cell polarity and cyst morphogenesis were therefore the same in cells

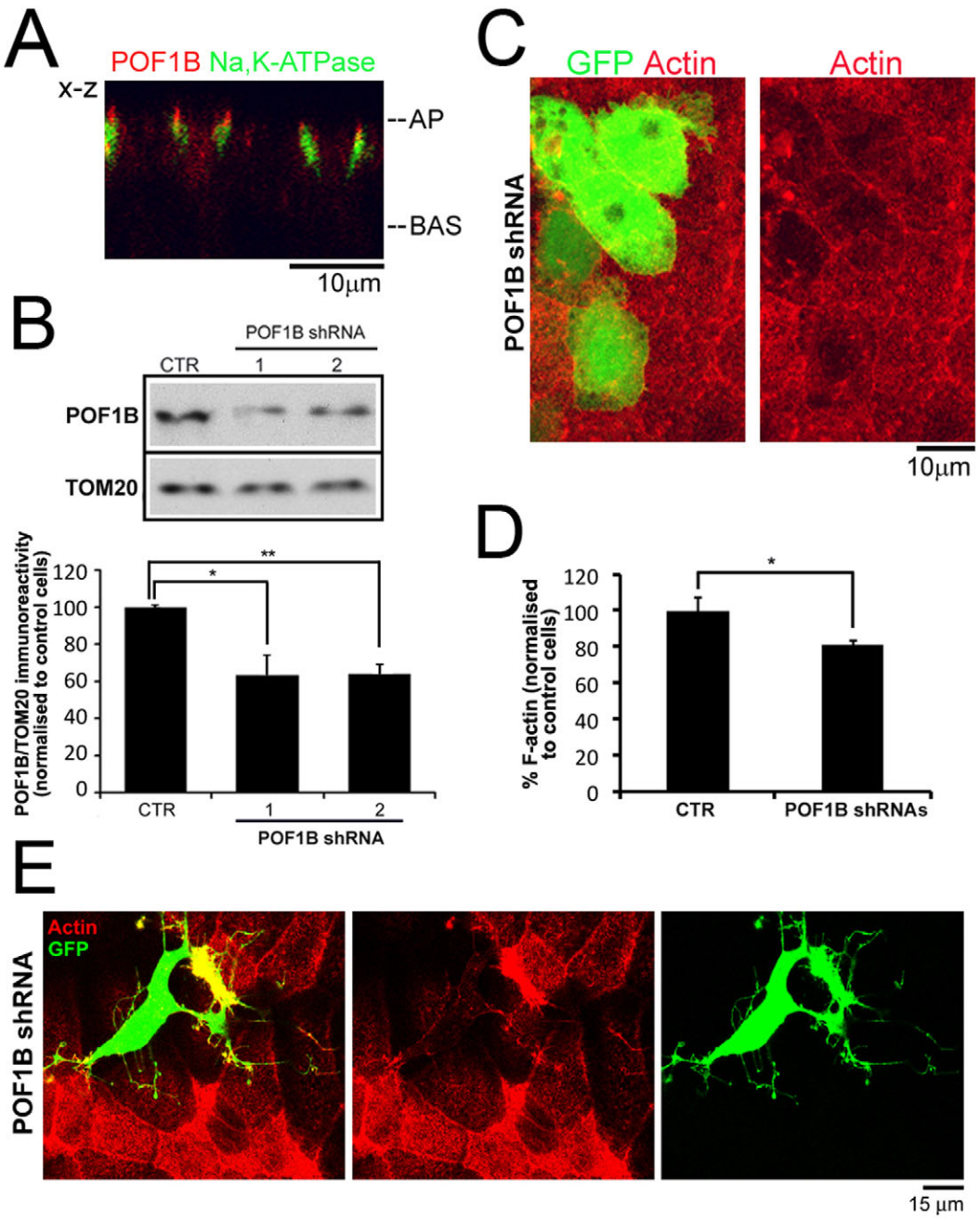

Fig. 5. POF1B silencing in human intestinal Caco-2 cells. (**A**) Vertical confocal section (x-z) of fully polarised Caco-2 cells grown on Transwell filters for>7 days and stained for POF1B (red) and Na^+/K^+-ATPase (green). AP: apical surface; BAS: basal surface. (**B**) A representative western blot analysis is shown. Ten μg of total protein extracts from Caco-2 cells transiently transfected with the empty pSUPER vector (CTR) or with the vector containing shRNAs (1 and 2) were probed for POF1B expression, and the mitochondrial marker TOM20 as a loading control. The graph shows the POF1B expression level in silenced cells normalised to control cells (n=4). *P<0.05; **P<0.01. (**C**) Caco-2 cells transiently transfected with POF1B shRNA (green) were stained with labelled phalloidin (actin). A merged image (left) and its corresponding individual staining for F-actin (right) are shown. (**D**) F-actin content comparison in cells transiently transfected with POF1B shRNAs compared to the empty vector (set to 100%), as quantified by FACS analysis. Data represent mean ± s.e.m. of two independent experiments performed with shRNA1 and 2. *P<0.05. (**E**) Caco-2 cells transiently expressing POF1B shRNA (green) cultured for >5 days after transfection were stained with phalloidin (red).

overexpressing the WT and in untransfected cells examined over the same time period (Fig. 7B). Interestingly, Mut cyst defects were less noticeable after 6 days or more in culture, although the lumens still appeared to be collapsed, as shown by analysis of the circularity index (Akao et al., 2003) and gp135 staining (Fig. 7B–D). Misoriented cell division is therefore associated with an alternative mechanism of cyst lumen formation: instead of a single lumen enlarging as the cells divide and cysts grow, cells can first form multiple lumens that eventually generate a single collapsed lumen.

The altered mechanism of formation of the cyst lumens, however, did not associate with defects in cell polarity, because

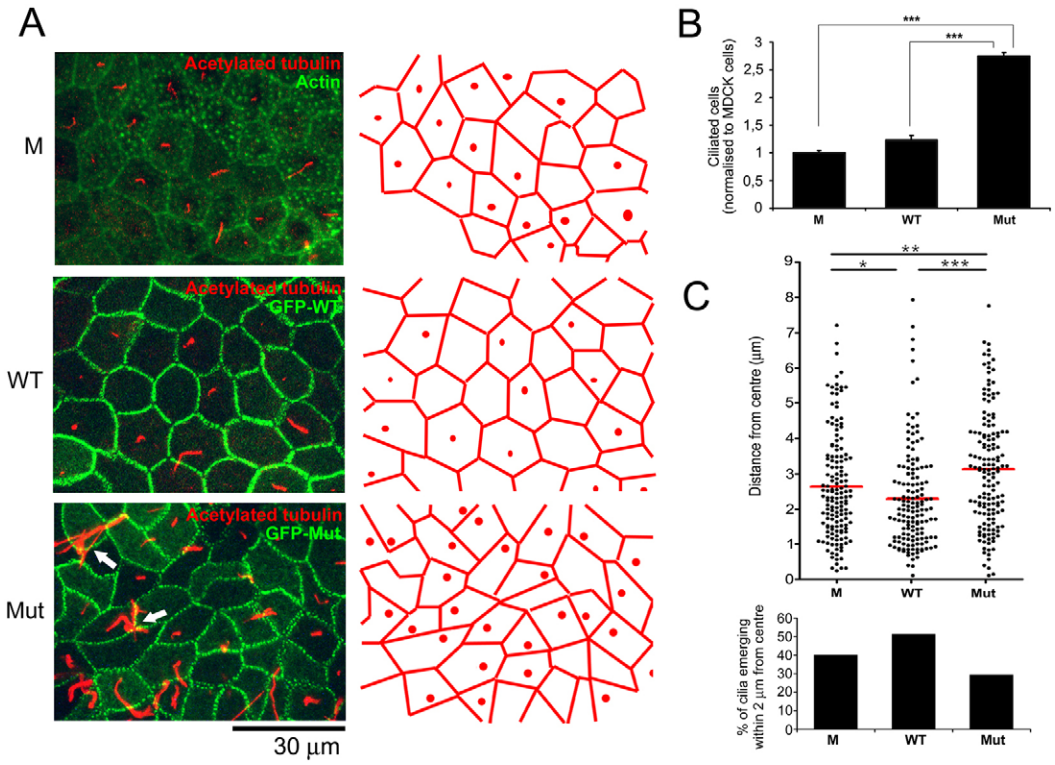

Fig. 6. Defects in ciliogenesis in cell lines expressing POF1B R329Q. Cells grown confluent for>4 days in Transwell filters were stained for the indicated markers. (**A**) Confocal z-stack projections of horizontal sections of cell monolayers in control MDCK cells (M) and MDCK cells expressing GFP-POF1B (WT) or GFP–POF1B R329Q (Mut) stained with acetylated tubulin to visualise primary cilia (red), phalloidin in M or GFP in WT and Mut (green). The red masks representing the cell boundary and the base of primary cilia were obtained from confocal sections taken from the sub-apical region through the emergence of primary cilia. Arrows indicates interlaced cilia tips. (**B**) The number of ciliated cells in monolayers expressing WT or Mut was normalised to MDCK cells ($n=350$ for each cell line). (**C**) Scatter plot of the distance from cilia emergence and cell centre ($n=150$ for each cell line) measured using a macro developed in ImageJ. Red lines indicate mean values and dots indicate individual data points of the ciliated cells analysed. The lower histogram represents the percentage of the primary cilia emerging within 2 μm from the centre. The values are means ± s.e.m. from three independent experiments performed with two stable clones for each transfectant. *$P<0.05$; **$P<0.01$; ***$P<0.001$.

the polarity markers β-catenin and gp135 were localised normally to cell–cell contacts and the surface facing the abnormal lumens, respectively, in Mut cysts (Fig. 7B, see apical staining in *x–y* and *x–z* sections). Mut expression therefore affects processes, such as cystogenesis and ciliogenesis, that are strictly related to tissue polarity, rather than cell polarity.

Discussion

POF1B is a candidate gene for premature ovarian failure that is highly and specifically expressed in polarised epithelia. Very little is known about the function of this gene, but its expression before the generation of the epidermal permeability barrier and its localisation to the junctional domain of epithelial tissues have led to the hypothesis that POF1B has a role in epithelial polarity (Rizzolio et al., 2007). Extending this hypothesis, the overall findings of this study converge to indicate that POF1B is involved in the organisation of a regular array of polarised cells, through the stabilisation of F-actin, rather than in the definition of apico-basal polarity. In particular, our data indicate that TJs, harbouring POF1B, are crucial structures that regulate monolayer polarity.

We found that the R329Q variant failed to accumulate in TJs of MDCK cells; however, this mislocalisation did not induce evident alterations in TJs or in the apico-basal polarity of these cells, as confirmed by the proper localization of TJ and polarity markers and a normal ultrastructure. Only the mechanism of TJ formation appeared altered in Mut cells (absence of a TER peak), and this defect might be explained by a difficulty in synchronising the formation of TJs owing to the irregular polygonal shape and sides of different length of the Mut cells. Alternatively, because of the important role of claudins in determining the TER value, it is also possible that downregulation of claudin-2 might at least contribute to the lack of a TER peak in Mut cells, although the unaffected permeability properties of these cells might suggest that other claudins compensate for the claudin-2 defect.

It is known that a regular cell shape (as defined by the polygonal nature of the cells in two dimensions) is crucial for the formation of epithelial polarised tissues. In agreement with this knowledge, we observed that the geometry of the monolayer of dysmorphic cells expressing the R329Q variant of POF1B was disturbed and even acquired a pseudostratified appearance when analysed by electron microscopy.

Cell shape is linked to the correct organisation of the actin cytoskeleton, a process that was altered in cells expressing the R329Q variant (lower fluorescence at the cell–cell contacts, lower F-actin to G-actin ratio and content of F-actin/cell) and in Caco-2 cells silenced for POF1B (decreased F-actin content and

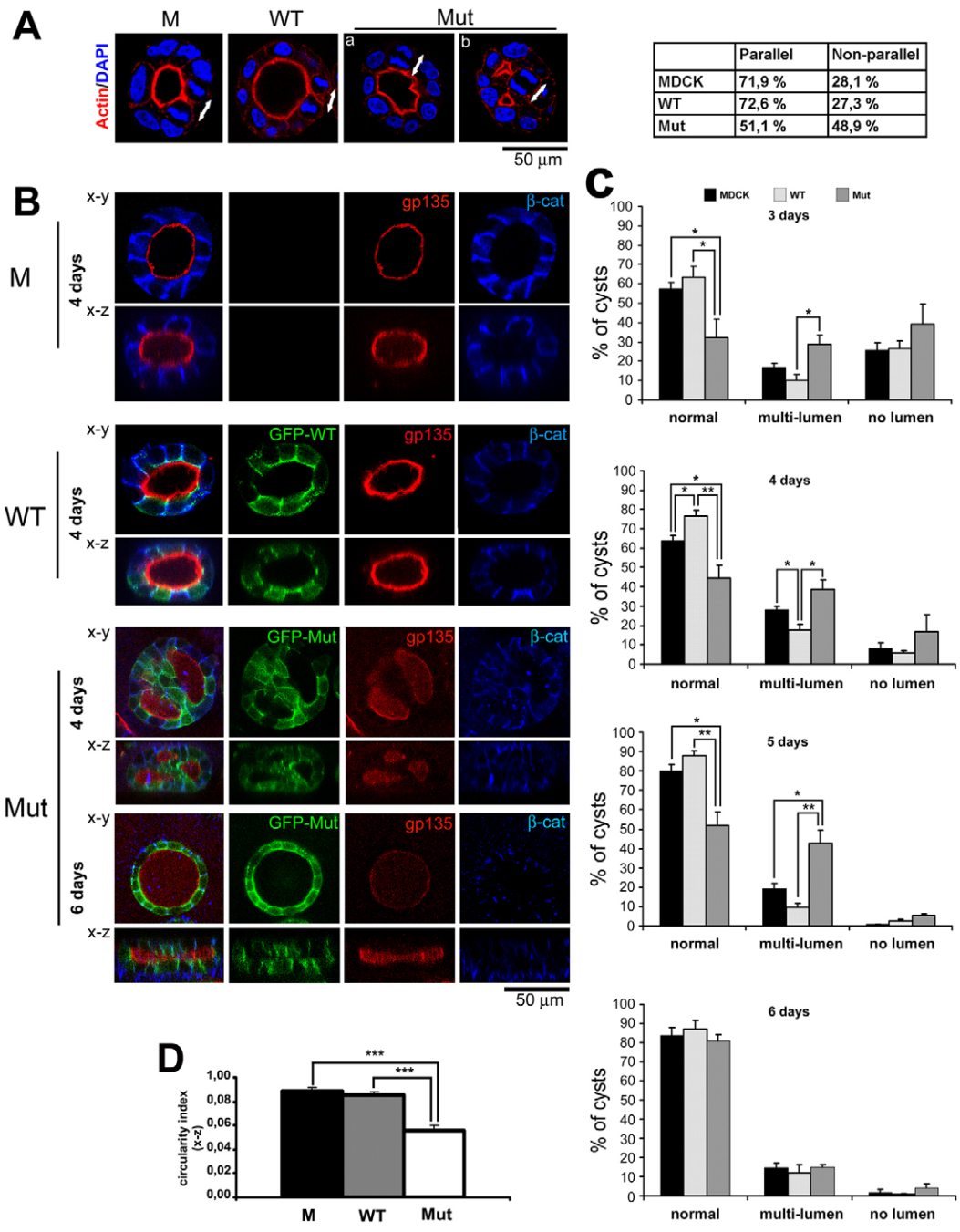

	Parallel	Non-parallel
MDCK	71,9 %	28,1 %
WT	72,6 %	27,3 %
Mut	51,1 %	48,9 %

Fig. 7. Altered mechanism of cystogenesis in cells expressing POF1B R329Q. Single cells were seeded in an extracellular matrix (Matrigel) and grown for the indicated time. The cysts were fixed in 4% paraformaldehyde, permeabilised, stained for the indicated marker, and analysed by laser confocal microscopy. The confocal sections were taken at the middle region of the cysts. (**A**) Representative images (red, F-actin; blue, DAPI) of 4-day-old cysts; the arrows represent the direction of mitotic division. Two examples of Mut cysts showing misoriented division in a single lumen (a) and in a multilumen (b) cyst. Quantification of the direction of mitotic division is shown in the right (n>80 for each cell line). Experiments were performed in triplicate with at least two stable clones for each transfectant. (**B**) Cyst polarisation was assessed by the extent of lumen formation and by staining for the gp135 apical marker (red) and the β-catenin lateral marker (blue) in horizontal (x–y) and vertical (x–z) confocal sections. (**C**) Quantitative analysis of cyst morphology in control (M), GFP–POF1B (WT) or GFP–POF1B R329Q (Mut) cell lines cultured for 3–6 days. The values are the percentage of cysts with the indicated lumen morphology (n=100 cysts for each cell line). (**D**) Quantitative analysis showing the circularity index of lumens of cysts in cells cultured for more than 6 days stained with Texas Red phalloidin (n=28 for each cell line). (C,D) Data are the means ± s.e.m. of three independent experiments using two stable clones. *P<0.05; **P<0.01; ***P<0.001.

altered cell shape). In sharp contrast, the overexpression of WT POF1B did not alter the cell geometry or the F-actin content, and the F-actin to G-actin ratio even increased in these cells. Although this chain of events is clear, its remote cause is an open question. Regulation of TJ stability has a key role in epithelial polarity (Van Itallie et al., 2009), thus the simple absence of POF1B variant from these junctions might prevent F-actin stabilisation, thus destabilising them. In this respect, in vitro experiments have shown that POF1B R329Q presents a lower affinity for F-actin than WT POF1B (Lacombe et al., 2006). In accordance with this finding, we observed a larger colocalisation of F-actin with POF1B at cell–cell contacts of WT compared with Mut cells. It is therefore possible that the stabilisation of the cytoskeleton at TJs requires a direct interaction between F-actin and POF1B. In line with this possibility, the altered shape of Mut cells might be due to the lack of localisation of Mut to tight junctions and its diffuse localisation along the entire lateral surface; these defects together with a decreased affinity for F-actin might account for the decreased enrichment of the actin cytoskeleton at the junctional surface, leading to irregularity in the cell geometry. Alternatively, the effect should involve a functional interaction of POF1B with some partners residing at TJs, raising questions about the number of partners and the interactions of POF1B in these junctions. In this regard, it must

be noted that POF1B contains a coiled-coil domain homologous to the rod domain of a myosin (Lacombe et al., 2006), and common to motor and skeletal proteins. This domain might determine the protein's oligomerisation state, rigidity and ability to function as a molecular recognition system (Burkhard et al., 2001), raising the possibility that oligomerisation of the overexpressed mutant with the endogenous protein interferes with POF1B function in F-actin stabilisation, thus conferring to the mutant a dominant-negative function that might also account for the decreased expression of gp135 and claudin-2, because their expression and/or localisation depends on the actin cytoskeleton (Ojakian and Schwimmer, 1988; Bruewer et al., 2004).

There is accumulating evidence that regulation of actin dynamics is a main function of PCP signalling, which acts through small GTPases of the RhoA family (Kim and Han, 2005; Ybot-Gonzalez et al., 2007), a formin-homology (FH)-domain protein that binds actin and nucleates filament polymerisation (Habas et al., 2001; Liu et al., 2008), and a myosin that controls the cytoskeletal reorganisation of cellular junctions during epithelial morphogenesis (Bertet et al., 2004; Rauzi et al., 2010). In support of a role for POF1B in epithelial PCP, we have also provided data showing altered emergence of cilia docking sites in 2D cultures and misorientation of mitotic division in 3D cultures of Mut cells. Interestingly, many polarity proteins localised to TJs have been implicated in mitotic orientation during epithelial cell division (Hao et al., 2010; Qin et al., 2010; Zheng et al., 2010) and ciliogenesis in polarized epithelia (Sfakianos et al., 2007). Several studies have highlighted a primary role for the actin cytoskeleton in centriole positioning (Vaughan and Dawe, 2011) and the described defects in ciliogenesis and cystogenesis might be due to random positioning of centrioles or centriole analogous structures (i.e. basal bodies), controlling the symmetrical cell division in proliferating cells or the cilium emergence in fully polarised cells, respectively.

Polarised epithelial tissues regulate ovarian function in a number of ways, and a key organiser of actin dynamics, the formin-related gene *DIAPH2* (Diaphanous-related formin-2) (Bione et al., 1998), which also maps to the X chromosome critical region for ovarian function, is another candidate gene for POF. The decision of developing follicles to continue growing and eventually to ovulate or to undergo atresia mainly depends on the intimate relationship between oocytes and the surrounding highly specialised epithelial granulosa cells. During the course of this development, granulosa cells proliferate, thus contributing to follicle enlargement (Jablonka-Shariff et al., 1996; Hirshfield, 1997; Albertini et al., 2001) and, by converting testosterone to oestrogen, these cells are responsible for the increased level of hormone in the bloodstream. Thus, the low levels of oestrogens in POF might be explained by a defect in granulosa cell division. Moreover, ovarian epithelia and the secretory epithelium of the ovarian oviduct have primary cilia, and ovulation was impaired in transgenic mice in which ovarian primary cilia were deleted (Johnson et al., 2008), indicating a crucial role for this organelle in the ovarian functions.

In conclusion, our data provide evidence of a major role for POF1B in controlling cell shape and monolayer organisation, which is a key feature that drives morphogenesis during development and is critical for organ function. Moreover, we have shown that TJs are crucial sites in determining polarisation of monolayers.

Materials and Methods

Constructs

Full-length human *POF1B*, corresponding to amino acids 3–589 of POF1B (NCBI database accession # Q8WVV4), was fused to the C-terminus of GFP by subcloning the PCR product into the *Xho*I–*Bam*HI restriction fragment of the mammalian expression vector pAcGFP1-C1 (Clonetech, CA). POF1B R329Q was generated by means of QuikChange Site-directed Mutagenesis (Stratagene, CA) polymerase chain reaction (PCR) using GFP–POF1B as the template and complementary oligonucleotides containing AG instead of GA at position 986–987 of the coding sequence (oligo upper 5′-GTCTGATAAGTCACTCC**AG**CTAGTGCTGTCCAC-3′ and the complementary oligo lower). A *Bpm*I site was created by the substitution and used to identify the mutagenised product.

To create the shRNA constructs, two 19-base pair sites within human *POF1B* were chosen using on-line biocomputer tools, and pairs of complementary oligonucleotides containing the following target sequences were synthesised by Sigma: 5′-GCAAGGACTTCAAGACTCA-3′ (shRNA1), corresponding to the amino acids 375–381 in the coiled-coil domain region, and 5′-AATGCCATCATCACATTAT-3′ (shRNA2), corresponding to the amino acids 181–187. These sequences did not have any significant homology to other genes in the human genome database. The forward and reverse oligos were annealed and cloned into *Bgl*II–*Xho*I restriction sites of the pSUPER.gfp/neo RNAi system (OligoEngine), and the resulting plasmid was amplified. All of the plasmid sequences were verified by means of automated sequencing to exclude unwanted substitutions.

Cell culture and transfection

MDCK (strain II) cells were cultured and stably transfected using the Ca-PO_4 method as previously described (Perego et al., 1999). The stable cell lines were selected on the basis of growth in the antibiotic G418 (0.6 mg/ml) (Sigma), and the expression of the constructs was assessed by fluorescence microscopy and western blotting. Four cell lines expressing the full-length protein (WT 5, 7, 10 and 13) and three cell lines expressing the R329Q variant (Mut 5, 6 and 12) were chosen on the basis of their homogeneity and levels of expression, most of the figures were obtained with WT 13 and Mut 5 unless otherwise indicated, and results from at least two clones are presented.

For morphological and functional (transepithelial electrical resistance, TER and Ca^{2+} switch) studies, the MDCK cell lines were seeded at a density of 2.5×10^5 cells/cm^2 onto Transwell filter inserts (0.4 μm pore size; Corning Costar, Sigma) and analysed for >3 days unless otherwise indicated. For the biochemical assays, the cells were plated at the same density on Iwaki or Falcon tissue culture dishes and used 3 days or more after plating unless otherwise indicated.

Organotypical 3D MDCK cell cultures were used for cyst formation as previously described (Vieira et al., 2006), the cultures grown for the time indicated were then fixed for 1 hour in 4% paraformaldehyde. Caco-2 cells were cultured in DMEM (Dulbecco's Modified Eagle Medium) supplemented with 1% L-glutamine, 1% penicillin-streptomycin and 10% fetal bovine serum (Sigma) at 37℃ and 5% CO_2, and transiently transfected using Fugene HD (Promega, Madison, WI) according to the manufacturer's protocol.

Calcium-switch experiments

For the calcium-switch protocol, the original method (Cereijido et al., 1978) was modified as follows: cell lines grown to confluency (2.5×10^5 cells/cm^2) on Transwell filter inserts (0.4 μm pore size; 12 mm diameter; Corning Costar) for >4 days (steady-state TER=50–60 ohm × cm^2) were incubated in calcium-free DMEM (Gibco) supplemented with 1% L-glutamine (Sigma) and calcium to a final concentration of 5 μM for 2 hours (TER=0). The cells were then grown in complete medium (1.8 mM Ca^{2+}) for 24 hours, and cell–cell contact formation was assessed at the indicated time by measuring TER.

Detergent extraction experiments

Detergent extraction experiments were carried out as described (Blikstad and Carlsson, 1982). Cells were treated for 30 minutes using extraction buffer (1% Triton X-100, 100 mM NaF, 50 mM KCl, 2 mM $MgCl_2$, 1 mM EGTA, 10 mM KPO_4, pH 7.5, 0.5 M sucrose) supplemented with PMSF and protease cocktail inhibitor (Sigma) to block the partial depolymerisation of actin seen in other buffers. After extraction, the cell extracts (G-actin fraction) were centrifuged at 13,000 ***g*** for 20 minutes, cell matrices (F-actin fraction) were collected by scraping the dish in 0.1 ml extraction buffer with a rubber policeman, and both fractions were solubilised in 0.1 ml sodium dodecyl sulfate (SDS) denaturation buffer and equal volumes of each fraction were analysed by immunoblotting for actin content.

F-actin FACS assay

Cells were trypsinised and fixed in 4% paraformaldehyde in PBS for 5 minutes before and after permeabilisation. Cells were stained with FITC-phalloidin (Jackson ImmunoResearch, PA) to detect F-actin. For all samples, 10,000 gated cells were analysed, and the mean F-actin content, as determined by the phalloidin staining, was quantified using the Cell Quest software system in FACSCalibur flow cytometer

(Becton Dickinson, San Jose). The values were expressed as percentage relative to untransfected MDCK or Caco-2 cells transfected with the empty vector.

Antibodies

The commercial primary antibodies were monoclonal mouse anti-β-catenin (BD), anti-JAM1 BV16 (Cell Science, MA), anti-claudin-1, 2 and anti-ZO-2 (Zymed Laboratories, San Francisco, CA), anti-GFP (MBL, Eppendorf, Woods Hole, MA and Hamburg, Germany), anti-actin and anti-acetylated tubulin (Sigma) and rabbit polyclonal anti-Par3 (Upstate, Billerica, MA). The rabbit polyclonal antibody against mouse LIN7A and human POF1B were raised against the corresponding fusion proteins (Perego et al., 2002; Rizzolio et al., 2007), and the rabbit polyclonal antibodies against α1 Na^+/K^+-ATPase and β-catenin were raised against specific peptides (Pietrini et al., 1992; Perego et al., 2002). The hybridoma cell line 3F2-secreting antibodies against gp135 were kindly provided by George K. Ojakian (Ojakian and Schwimmer, 1988).

Immunoblotting

Cell extracts were solubilised in sodium dodecyl sulfate (SDS) denaturation buffer. Equal amounts of total cell extract proteins (evaluated using Lowry's method) (Lowry et al., 1951) were separated on SDS-PAGE and transferred to nitrocellulose membranes. The blots were probed using the appropriate primary antibodies, followed by peroxidase-conjugated anti-rabbit or anti-mouse immunoglobulin G (Sigma) as secondary reagents, and visualised by means of an ECL Western blotting detection system (Perkin-Elmer Life Science, Waltham, MA). Signal intensity was quantified densitometrically using NIH ImageJ.

Light and immunofluorescence microscopy

Cells grown on glass coverslips or Transwell filters were fixed with 4% paraformaldehyde and permeabilised with 0.5% Triton X-100. Staining with the indicated primary antibodies was followed by incubation with Rhodamine- or Cy5-labelled rabbit and mouse secondary antibodies (Jackson Immunoresearch, Suffolk, UK). Texas-Red-labeled phalloidin (Molecular Probes, Eugene, OR) was used to detect filamentous actin. Samples were mounted using Vectashield (VectorLabs) containing DAPI for nuclei and antifade reagent. The images were acquired using a Bio-Rad MRC-1024 confocal microscope.

Sections of the frozen unfixed human jejunum (6 μm thick) were flattened over a gelatin-coated glass slide, fixed with acetone for 3 seconds and allowed to dry out overnight at room temperature. Sections were permeabilised with 0.5% Triton X-100, incubated overnight at 4℃ with primary antibodies, washed and incubated for 1 hour at room temperature with secondary antibodies.

Electron microscopy

Cells grown on Transwell filters were fixed in 2% (v/v) glutaraldehyde in 0.1 M cacodylate buffer, pH 7.4, and post-fixed with 1% (w/v) OsO_4 in 0.1 M cacodylate buffer. The samples were then stained en bloc, dehydrated in ethanol and embedded in EPON 812 (Fluka, Buchs, Switzerland) following standard procedures. Ultrathin sections were examined using a Philips CM10 transmission electron microscope (TEM).

Transepithelial electrical resistance

TER was determined using an Electrical Resistance System (Millicell-ERS; Millipore, San Francisco, CA). The TER values were obtained by subtracting the contributions of the filter (no cells) and bathing solution and were expressed as ohms × cm^2 (Balda et al., 1996), following the manufacturer's instructions. Three experiments each one with three parallel filters from control and transfected cell lines were measured for each time point.

Image and statistical analysis

Approximate values of angles at multiple cell-to-cell contacts, as well as the distance between the cell centre and the point of emergence of the primary cilium, were calculated by means of semi-automatic, custom procedures using the freely available ImageJ program. To obtain values of angles from a planar image of MDCK cells, we constructed binary maps of cell locations manually drawing the cell contours on an image. This image was then used as input for an ImageJ macro, which used it to identify cells, cell corners and internal angles. Centroids were calculated using ImageJ measurement functions and represented the average of the x and y coordinates of all of the pixels assigned to a cell. To obtain distances from cell centre and points of cilium emergence, we used stacks obtained by z-series of polarized cultures of MDCK cells. A binary map of cell locations was constructed by manually drawing cell contours, as observed in the most apical portion of the stack. This image, and the stack, were then used as inputs for a second ImageJ macro, which used the map to identify cells and cell centroids and used the stack to recognise the point of emergence of every cilium. The aforementioned procedures were validated manually. Detailed descriptions of the developed macros are available upon request.

The length of cell sides and orientation of mitotic division were calculated manually by considering the distance between two corners along the connecting cell wall and the position of mitotic chromosomes relative to the apical luminal surface, respectively. The 3D image reconstructions were conducted using z-series of MDCK cell lines (WT13 and Mut5) taken with the same confocal parameters and processed with the 'make isotropic' plug-in and volume reconstruction rendering (ImageJ 3D viewer). Colocalisation of POF1B with F-actin was quantified by Manders' colocalisation coefficients (ImageJ JACoP plug-in analysis) (Bolte and Cordelieres, 2006).

The circularity of the cyst lumens was determined using the formula $4\pi(\text{area})/(\text{perimeter})^2$; the values obtained with this formula are closer to 1.0 as a profile approaches circularity (Akao et al., 2003). All quantitative data are presented as mean ± s.e.m. Multiple comparisons among groups were carried out by Student's t-test using Prism software (GraphPad PrismTM software). Statistical analyses were obtained from three different experiments performed with at least two clones for each transfectant, $^*P<0.05$, $^{**}P<0.01$ and $^{***}P<0.001$.

Acknowledgements

V.P. was supported by a fellowship from Fondazione Fratelli Confalonieri. We thank Emilio Berti (University of Milano-Bicocca) for providing human tissues and discussions, and Kevin Smart for his help in preparing the text.

Supplementary material available online at
http://jcs.biologists.org/lookup/suppl/doi:10.1242/jcs.088237/-/DC1

References

Akao, M., O'Rourke, B., Kusuoka, H., Teshima, Y., Jones, S. P. and Marban, E. (2003). Differential actions of cardioprotective agents on the mitochondrial death pathway. *Circ. Res.* **92**, 195-202.

Albertini, D. F., Combelles, C. M., Benecchi, E. and Carabatsos, M. J. (2001). Cellular basis for paracrine regulation of ovarian follicle development. *Reproduction* **121**, 647-653.

Balda, M. S., Whitney, J. A., Flores, C., Gonzalez, S., Cereijido, M. and Matter, K. (1996). Functional dissociation of paracellular permeability and transepithelial electrical resistance and disruption of the apical-basolateral intramembrane diffusion barrier by expression of a mutant tight junction membrane protein. *J. Cell Biol.* **134**, 1031-1049.

Bertet, C., Sulak, L. and Lecuit, T. (2004). Myosin-dependent junction remodelling controls planar cell intercalation and axis elongation. *Nature* **429**, 667-671.

Bione, S., Sala, C., Manzini, C., Arrigo, G., Zuffardi, O., Banfi, S., Borsani, G., Jonveaux, P., Philippe, C., Zuccotti, M. et al. (1998). A human homologue of the *Drosophila melanogaster* diaphanous gene is disrupted in a patient with premature ovarian failure: evidence for conserved function in oogenesis and implications for human sterility. *Am. J. Hum. Genet.* **62**, 533-541.

Bione, S., Rizzolio, F., Sala, C., Ricotti, R., Goegan, M., Manzini, M. C., Battaglia, R., Marozzi, A., Vegetti, W., Dalpra, L. et al. (2004). Mutation analysis of two candidate genes for premature ovarian failure, DACH2 and POF1B. *Hum. Reprod.* **19**, 2759-2766.

Blikstad, I. and Carlsson, L. (1982). On the dynamics of the microfilament system in HeLa cells. *J. Cell Biol.* **93**, 122-128.

Bolte, S. and Cordelieres, F. P. (2006). A guided tour into subcellular colocalization analysis in light microscopy. *J. Microsc.* **224**, 213-232.

Bruewer, M., Hopkins, A. M., Hobert, M. E., Nusrat, A. and Madara, J. L. (2004). RhoA, Rac1, and Cdc42 exert distinct effects on epithelial barrier via selective structural and biochemical modulation of junctional proteins and F-actin. *Am. J. Physiol. Cell Physiol.* **287**, C327-C335.

Burkhard, P., Stetefeld, J. and Strelkov, S. V. (2001). Coiled coils: a highly versatile protein folding motif. *Trends Cell Biol.* **11**, 82-88.

Carthew, R. W. (2005). Adhesion proteins and the control of cell shape. *Curr. Opin. Genet. Dev.* **15**, 358-363.

Cereijido, M., Robbins, E. S., Dolan, W. J., Rotunno, C. A. and Sabatini, D. D. (1978). Polarized monolayers formed by epithelial cells on a permeable and translucent support. *J. Cell Biol.* **77**, 853-880.

Coulam, C. B., Adamson, S. C. and Annegers, J. F. (1986). Incidence of premature ovarian failure. *Obstet. Gynecol.* **67**, 604-606.

Davis, C. J., Davison, R. M., Payne, N. N., Rodeck, C. H. and Conway, G. S. (2000). Female sex preponderance for idiopathic familial premature ovarian failure suggests an X chromosome defect: opinion. *Hum. Reprod.* **15**, 2418-2422.

de Moraes-Ruehsen, M. and Jones, G. S. (1967). Premature ovarian failure. *Fertil. Steril.* **18**, 440-461.

Habas, R., Kato, Y. and He, X. (2001). Wnt/Frizzled activation of Rho regulates vertebrate gastrulation and requires a novel Formin homology protein Daam1. *Cell* **107**, 843-854.

Hao, Y., Du, Q., Chen, X., Zheng, Z., Balsbaugh, J. L., Maitra, S., Shabanowitz, J., Hunt, D. F. and Macara, I. G. (2010). Par3 controls epithelial spindle orientation by aPKC-mediated phosphorylation of apical pins. *Curr. Biol.* **20**, 1809-1818.

Hirshfield, A. N. (1997). Overview of ovarian follicular development: considerations for the toxicologist. *Environ. Mol. Mutagen.* **29**, 10-15.

Jablonka-Shariff, A., Reynolds, L. P. and Redmer, D. A. (1996). Effects of gonadotropin treatment and withdrawal on follicular growth, cell proliferation, and atresia in ewes. *Biol. Reprod.* **55**, 693-702.

Jaffe, A. B., Kaji, N., Durgan, J. and Hall, A. (2008). Cdc42 controls spindle orientation to position the apical surface during epithelial morphogenesis. *J. Cell Biol.* **183**, 625-633.

Johnson, E. T., Nicola, T., Roarty, K., Yoder, B. K., Haycraft, C. J. and Serra, R. (2008). Role for primary cilia in the regulation of mouse ovarian function. *Dev. Dyn.* **237**, 2053-2060.

Kim, G. H. and Han, J. K. (2005). JNK and ROKalpha function in the noncanonical Wnt/RhoA signaling pathway to regulate *Xenopus* convergent extension movements. *Dev. Dyn.* **232**, 958-968.

Kim, J., Lee, J. E., Heynen-Genel, S., Suyama, E., Ono, K., Lee, K., Ideker, T., Aza-Blanc, P. and Gleeson, J. G. (2010). Functional genomic screen for modulators of ciliogenesis and cilium length. *Nature* **464**, 1048-1051.

Krauss, C. M., Turksoy, R. N., Atkins, L., McLaughlin, C., Brown, L. G. and Page, D. C. (1987). Familial premature ovarian failure due to an interstitial deletion of the long arm of the X chromosome. *N. Engl. J. Med.* **317**, 125-131.

Lacombe, A., Lee, H., Zahed, L., Choucair, M., Muller, J. M., Nelson, S. F., Salameh, W. and Vilain, E. (2006). Disruption of POF1B binding to nonmuscle actin filaments is associated with premature ovarian failure. *Am. J. Hum. Genet.* **79**, 113-119.

Liu, W., Sato, A., Khadka, D., Bharti, R., Diaz, H., Runnels, L. W. and Habas, R. (2008). Mechanism of activation of the Formin protein Daam1. *Proc. Natl. Acad. Sci. USA* **105**, 210-215.

Lowry, O. H., Rosebrough, N. J., Farr, A. L. and Randall, R. J. (1951). Protein measurement with the Folin phenol reagent. *J. Biol. Chem.* **193**, 265-275.

Mattison, D. R., Evans, M. I., Schwimmer, W. B., White, B. J., Jensen, B. and Schulman, J. D. (1984). Familial premature ovarian failure. *Am. J. Hum. Genet.* **36**, 1341-1348.

Mostov, K., Brakeman, P., Datta, A., Gassama, A., Katz, L., Kim, M., Leroy, P., Levin, M., Liu, K., Martin, F. et al. (2005). Formation of multicellular epithelial structures. *Novartis Found. Symp.* **269**, 193-200; discussion **200-195**, 223-130.

Ojakian, G. K. and Schwimmer, R. (1988). The polarized distribution of an apical cell surface glycoprotein is maintained by interactions with the cytoskeleton of Madin-Darby canine kidney cells. *J. Cell Biol.* **107**, 2377-2387.

Perego, C., Vanoni, C., Villa, A., Longhi, R., Kaech, S. M., Frohli, E., Hajnal, A., Kim, S. K. and Pietrini, G. (1999). PDZ-mediated interactions retain the epithelial GABA transporter on the basolateral surface of polarized epithelial cells. *EMBO J.* **18**, 2384-2393.

Perego, C., Vanoni, C., Massari, S., Raimondi, A., Pola, S., Cattaneo, M. G., Francolini, M., Vicentini, L. M. and Pietrini, G. (2002). Invasive behaviour of glioblastoma cell lines is associated with altered organisation of the cadherin-catenin adhesion system. *J. Cell Sci.* **115**, 3331-3340.

Pietrini, G., Matteoli, M., Banker, G. and Caplan, M. J. (1992). Isoforms of the Na,K-ATPase are present in both axons and dendrites of hippocampal neurons in culture. *Proc. Natl. Acad. Sci. USA* **89**, 8414-8418.

Qin, Y., Meisen, W. H., Hao, Y. and Macara, I. G. (2010). Tuba, a Cdc42 GEF, is required for polarized spindle orientation during epithelial cyst formation. *J. Cell Biol.* **189**, 661-669.

Rauzi, M., Lenne, P. F. and Lecuit, T. (2010). Planar polarized actomyosin contractile flows control epithelial junction remodelling. *Nature* **468**, 1110-1114.

Riva, P., Magnani, I., Fuhrmann Conti, A. M., Gelli, D., Sala, C., Toniolo, D. and Larizza, L. (1996). FISH characterization of the Xq21 breakpoint in a translocation carrier with premature ovarian failure. *Clin. Genet.* **50**, 267-269.

Rizzolio, F., Bione, S., Villa, A., Berti, E., Cassetti, A., Bulfone, A., Tribioli, C. and Toniolo, D. (2007). Spatial and temporal expression of POF1B, a gene expressed in epithelia. *Gene Expr. Patterns* **7**, 529-534.

Rodriguez-Fraticelli, A. E., Vergarajauregui, S., Eastburn, D. J., Datta, A., Alonso, M. A., Mostov, K. and Martin-Belmonte, F. (2010). The Cdc42 GEF Intersectin 2 controls mitotic spindle orientation to form the lumen during epithelial morphogenesis. *J. Cell Biol.* **189**, 725-738.

Sfakianos, J., Togawa, A., Maday, S., Hull, M., Pypaert, M., Cantley, L., Toomre, D. and Mellman, I. (2007). Par3 functions in the biogenesis of the primary cilium in polarized epithelial cells. *J. Cell Biol.* **179**, 1133-1140.

Simons, M. and Mlodzik, M. (2008). Planar cell polarity signaling: from fly development to human disease. *Annu. Rev. Genet.* **42**, 517-540.

Singla, V. and Reiter, J. F. (2006). The primary cilium as the cell's antenna: signaling at a sensory organelle. *Science* **313**, 629-633.

Song, H., Hu, J., Chen, W., Elliott, G., Andre, P., Gao, B. and Yang, Y. (2010). Planar cell polarity breaks bilateral symmetry by controlling ciliary positioning. *Nature* **466**, 378-382.

Van Itallie, C. M., Fanning, A. S., Bridges, A. and Anderson, J. M. (2009). ZO-1 stabilizes the tight junction solute barrier through coupling to the perijunctional cytoskeleton. *Mol. Biol. Cell* **20**, 3930-3940.

Vaughan, S. and Dawe, H. R. (2011). Common themes in centriole and centrosome movements. *Trends Cell Biol.* **21**, 57-66.

Vieira, O. V., Gaus, K., Verkade, P., Fullekrug, J., Vaz, W. L. and Simons, K. (2006). FAPP2, cilium formation, and compartmentalization of the apical membrane in polarized Madin-Darby canine kidney (MDCK) cells. *Proc. Natl. Acad. Sci. USA* **103**, 18556-18561.

Ybot-Gonzalez, P., Savery, D., Gerrelli, D., Signore, M., Mitchell, C. E., Faux, C. H., Greene, N. D. and Copp, A. J. (2007). Convergent extension, planar-cell-polarity signalling and initiation of mouse neural tube closure. *Development* **134**, 789-799.

Zegers, M. M., O'Brien, L. E., Yu, W., Datta, A. and Mostov, K. E. (2003). Epithelial polarity and tubulogenesis in vitro. *Trends Cell Biol.* **13**, 169-176.

Zheng, Z., Zhu, H., Wan, Q., Liu, J., Xiao, Z., Siderovski, D. P. and Du, Q. (2010). LGN regulates mitotic spindle orientation during epithelial morphogenesis. *J. Cell Biol.* **189**, 275-288.